IOPscience iopscience.iop.org

Home Search Collections Journals About Contact us My IOPscience

Silicon oxynitride as a tunable optical material

This article has been downloaded from IOPscience. Please scroll down to see the full text article.

1994 J. Phys.: Condens. Matter 6 4961

(http://iopscience.iop.org/0953-8984/6/26/018)

View the table of contents for this issue, or go to the journal homepage for more

Download details:
IP Address: 171.66.16.147
The article was downloaded on 12/05/2010 at 18:45

Please note that terms and conditions apply.

J. Phys.: Condens. Matter 6 (1994) 4961–4970. Printed in the UK

Silicon oxynitride as a tunable optical material

S C Bayliss†§ and S J Gurman‡

† Department of Physics, Loughborough University of Technology, Loughborough LE11 3TU, UK

‡ Department of Physics and Astronomy, University of Leicester, Leicester LE1 7RH, UK

Received 14 January 1994, in final form 19 April 1994

Abstract. Thin disordered films of the ternary system SiO_xN_y with $0 < x < 2$ and $0 < y < 1.33$ have been sputtered reactively for optical and structural studies. Here we present structural information for these materials from EXAFS, from which it is found that the silicon oxynitride system is chemically ordered as expected. The optical tunability of this system has been determined from optical absorption, bandgap and refractive index measurements. We find that a specified bandgap with varying refractive index (or specified refractive index with tunable bandgap) is achievable within a restricted range of refractive index (or bandgap), for larger values of x and y. This conclusion from the experimental data is supported by bandgap and refractive index calculations using scaling theory.

1. Introduction

The technological importance of materials such as SiO_x and SiN_x arises from the tunability of their bandgaps, for example as boundary layers [1] and windows for solar cells [2, 3] and photodetectors [3]. By varying the composition the optical gaps of these alloys can be varied over a wide range to produce materials which can be semiconductors or insulators, with bandgaps from 1.1 to 10 eV for the sub-oxide and from 1.1 to 7 eV for the sub-nitride [4, 5]. In addition samples of any silicon-rich composition can be prepared by sputtering. Our interest in these alloy systems arises because the influence of intrinsic structural disorder on their dielectric properties can be investigated [4, 5].

With binary alloys we may tune the bandgap over a fairly wide range; however, we have no degree of freedom to vary other properties, such as the static refractive index $n(0)$ at constant bandgap. Ternary alloys give us this freedom, and we have prepared therefore a set of materials based on the silicon oxynitride system SiO_xN_y. This system has been studied previously in Loughborough [6] when growth conditions were investigated in order to tailor the transmission and refractive index properties of the films deposited. In this study thin films of SiO_xN_y with $0 < x < 2$ and $0 < y < 1.33$ have been sputtered reactively for both optical and structural studies, since it may be expected that the electronic properties of solids are closely linked to their structure, and in particular to the chemical bonding, and thus an understanding of the structure is necessary if the optical properties are to be fully understood. Here we present optical absorption, bandgap and refractive index data, and structural information from EXAFS. Calculations of static refractive index and optical bandgap, using scaling theory [7] based on a Phillips [8] and van Vechten [9] model for the susceptibility, are compared with the experimental data.

§ Present address: Department of Applied Physics, De Montfort University, Leicester LE1 9BH, UK.

0953-8984/94/264961+10$19.50 © 1994 IOP Publishing Ltd

2. Sample preparation

Samples of silicon oxynitride were deposited by DC unbalanced magnetron reactive sputtering, at a base pressure of $\sim 10^{-6}$ Torr. The plasma gas was argon at a partial pressure of 2 mTorr. Oxygen and nitrogen were used as reactive plasma gases, and control of the flow rates of the reactive gases was used to produce films of various compositions. Under these conditions a deposition rate of ~ 1 nm s^{-1} was achieved. A full description of the system used can be found in [6]. For this study 27 samples ~ 500 nm thick were deposited with various values of x and y to cover the entire composition ranges up to stoichiometry (i.e. $0 < x < 2$ and $0 < y < 1.33$). The films were deposited onto various substrates during the same deposition run, to enable optical and structural analyses to be made by a variety of experimental techniques.

The compositions of the samples were determined from EXAFS Si K-edge step heights, measured at the 2 GeV SERC Synchrotron Radiation Source (SRS) at Daresbury (see below), and from XPS core-level peak areas, using a VG Escalab. Results from the two methods were consistent within experimental error (±5% in both sets of measurements). The amount of impurities in the samples was found to be low, the most abundant unwanted species being argon at < 2%. Samples were also checked for amorphicity by transmission electron microscopy. In all cases the diffraction patterns showed the diffuse rings expected of a homogeneous amorphous material.

3. Structural measurements from EXAFS

EXAFS measurements on the silicon oxynitride were carried out at the SRS. The x-ray absorption was measured about the Si K edge (at ~ 1840 eV). Beam currents during data taking were typically between 150 and 250 mA. The experiments were performed on the SOXAFS beamline which has a Cr-plated mirror to focus the beam at the sample. The energy of the x-ray beam was defined using an InSb(111) double-crystal monochromator with harmonic rejection set at 70%. The incident beam intensity was monitored by an Al foil.

Absorption at the sample was measured by the electron drain current method, a modification of the total yield method [10]. Since this method measures the electron drain needed to earth the sample after photoelectron emission, a path is required for electrical conduction. Thin film samples for EXAFS were prepared on aluminium substrates and, to ensure good electrical connection, were dagged to the substrate holder using silver-loaded paint. The edges of the samples were also connected electrically to the substrate holder using a layer of this paint. The angle between the incident beam and the sample surface was approximately 90°.

The measured absorption spectra are proportional to the total absorption coefficient $\mu(E)$, and these data contain three types of information on the atomic and electronic subsystems in the sample. Firstly, since the drain current method samples only the first ~ 10 nm into the material, $\mu(E)$ contains no substrate contribution and thus the relative step heights in $\mu(E)$ contain information on the sample composition. In this work the relative silicon compositions have to be obtained using the atomic absorption coefficients of Viegele [11]. It should be noted that the percentage of argon in the samples was found by XPS to be sufficiently low (< 2%) that it could be neglected in these determinations of composition. Secondly, the region close to the absorption edge (XANES) effectively profiles the conduction band density of states, if a rigid filling of the states can be assumed to occur. Thirdly the EXAFS itself contains information on the atomic structure.

The absorption spectra were background subtracted using the EXBACK program [12]. The resulting EXAFS spectra χ were then analysed by a least-squares curve-fitting procedure, using fast curved wave theory [13], using the EXCURV90 program [12]. The structural parameters fitted were the coordination numbers of a particular atom type surrounding the central silicon atoms, the respective bondlengths, and the Debye–Waller factors. This latter term provides a description of the effects of thermal and static disorder on the interatomic distances. The analysis programs also allow us to determine the uncertainties in the fitted parameters corresponding to the 95% confidence region, i.e. the $\pm 2\sigma$ uncertainties where σ is the standard deviation. The electron scattering phase-shifts were calculated within the programme.

4. Experimental optical properties

Refractive indices and thicknesses were determined by ellipsometry using a Gaertner ellipsometer, and by use of interference fringes in the reflection and transmission data using the method of Cisneros *et al* [14]. Reflection and transmission were measured using both Hitachi U2000 and Perkin–Elmer 320 spectrometers in order to cover the wavelength range from 190 nm–3500 nm, and so provide a dispersion curve for each sample. These curves were then extrapolated using polynomial fits down to zero energy to obtain the static refractive indices. The optical absorption edges were also determined from the reflection and tranmission measurements, and were used to obtain values of the optical bandgap E_{04}, the photon energy at which the absorption coefficient has a value of 10^4 cm^{-1}.

5. Structural results

A typical phase-shift-corrected $k^3\chi(k)$ and its Fourier transform are shown in figure 1 for a-SiO_xN_y with $x = 1.0$ and $y = 0.7$. The Si–O and Si–N distances fitted are 1.62 and 1.74 ($\pm$0.02) Å respectively, very similar to the values found in the binary alloys. The noise level associated with the Si K-edge EXAFS spectra allowed a data range to ~ 15 Å^{-1} in most cases, and showed no evidence for second or higher shells, confirming that the samples were amorphous. In addition the films were found to be chemically ordered: in each case Si was found to be fourfold coordinated, and the data were consistent with N and O having respectively three and two Si nearest neighbours. As expected for a chemically ordered system each Si atom was found to be fourfold coordinated by only N and/or O atoms at stoichiometry. This was as found previously for the respective binary alloys [4, 5]. Indeed including a Si–Si shell in the fit to the dataset shown in figure 1 produced a Si–Si coordination of ~ 1.0 at a distance of 2.35 Å but did not improve the fit. The errors on the individual coordination numbers of the nitrogen and oxygen shells in the ternary compounds were, however, quite large, being about ± 1 to ± 2.

The Si–Si, Si–O and Si–N bond Debye–Waller factors in the ternary compounds, were, within error, constant throughout the composition ranges studied. The thermal contributions to the structural disorder have previously been determined for the bond types using a simple Einstein model [4, 5]. The three types of bond all showed a small static disorder in the bondlengths above the expected thermal disorder, that for the relatively strong and rigid Si–O bonds being less than for the Si–N bonds. It can also be seen in table 1 that, for both Si–Si and Si–N bond types, the static disorder is the same as for the respective binary alloys. In the binary alloys, however, Si–O bonds showed no static disorder. It is possible that

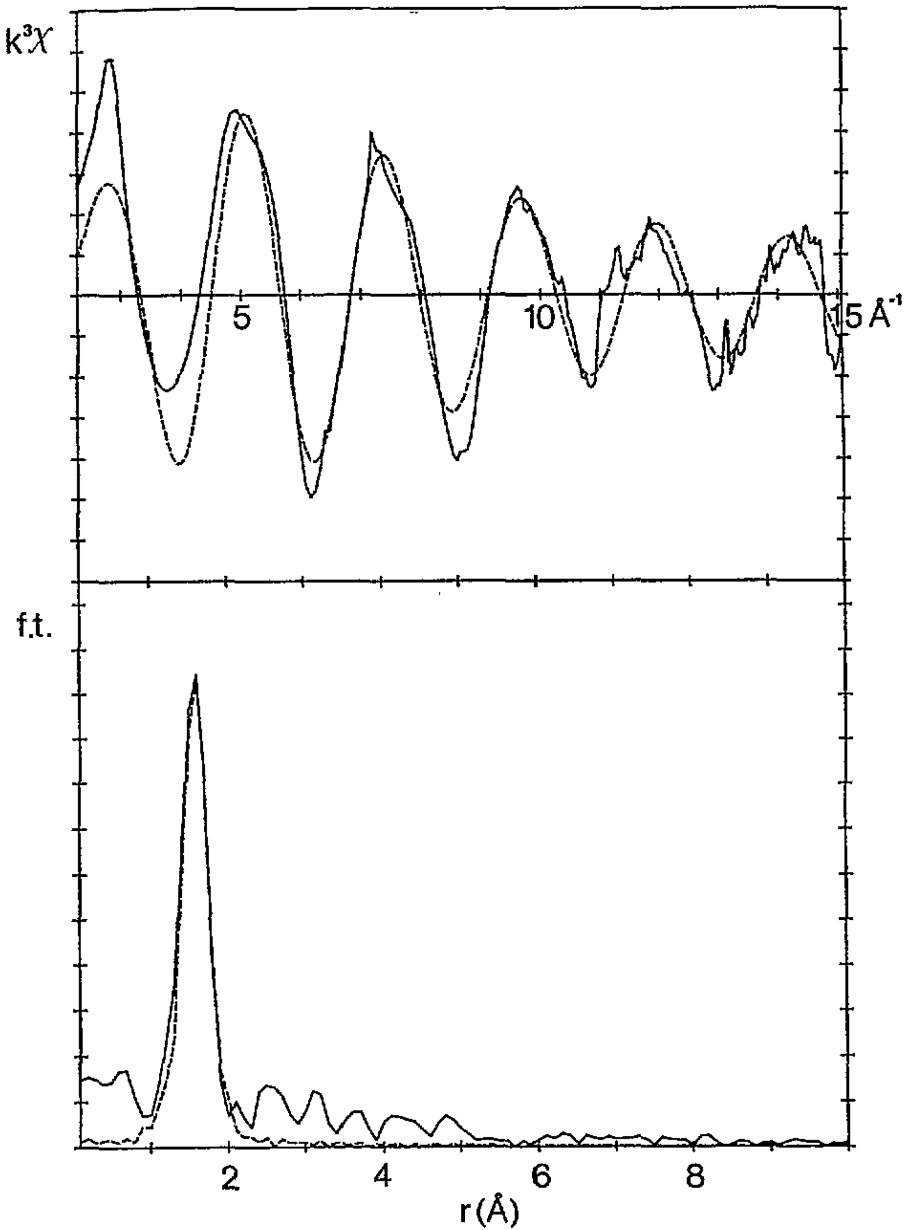

Figure 1. $k^3\chi(k)$ and the associated Fourier transform for a-SiO_xN_y with $x = 1.0$ and $y = 0.7$. Solid lines: experimental; dashed lines: theory.

the presence of excess configurational disorder in the ternary compound may have resulted from inhomogeneity of the conditions during deposition, resulting in intrinsic strain in the films.

A final note on the structure of silicon oxynitride concerns the work of Bustarret *et al* [15] who recently observed enhanced, visible luminescence in their as-deposited PECVD bulk a-Si:O:N:H films, similar to the luminescence found in porous silicon [16]. Bustarret

Table 1. Mean square deviations in bondlengths for a-SiO_xN_y system.

Thermal contributions		
Bond type	Vibration frequency	Deviation in bondlength
Si–Si	300 cm^{-1} stretch	0.004 $Å^2$
Si–O	1100 cm^{-1} stretch	0.001 $Å^2$
Si–N	900 cm^{-1} stretch	0.002 $Å^2$

Structural data from EXAFS	Bondlength deviation in	
Bond type	binary alloys	ternary alloy
Si–Si	0.006 ± 0.002 $Å^2$ (oxide) 0.006 ± 0.004 $Å^2$ (nitride)	0.007 ± 0.002 $Å^2$
Si–N	0.007 ± 0.004 $Å^2$	0.007 ± 0.003 $Å^2$
Si–O	0.001 ± 0.001 $Å^2$	0.004 ± 0.0015 $Å^2$

et al [15] ascribed the luminescence as possibly due to confinement of carriers in silicon chains or rings, due to the random structure expected in these materials. From our work it can be seen that sputtered films of silicon oxynitride are chemically ordered, with very few wrong bonds (if any) at stoichiometry. Although one should always be cautious when comparing structures of materials deposited by different methods, it is expected that the PECVD films should have an even lower density of wrong bonds. We therefore are led to the conclusion that there will be very little in the way of a silicon skeleton in the films of Bustarret *et al*, if the compositions are indeed effectively close to stoichiometry.

6. Optical results

Typical optical absorption edges for several silicon oxynitride samples are shown in figure 2. It can be seen that the edges are very similar in shape, and move monotonically to higher energies with increase in oxygen and/or nitrogen as expected. The bandgaps obtained from these edges therefore also show a monotonic shift to higher energies with increasing x and y. The experimental bandgaps obtained over the whole composition range for this ternary system are shown in figure 3. Here the dots show the compositions of the samples studied. The dashed lines indicate samples which show the same value of bandgap, the value itself being marked in italics. Samples which fall between the dashed lines show some intermediate value, but for reasons of clarity some of these individual values have been omitted. In order to make a comparison with our and other researchers' earlier work on binary alloys [4, 5, 17], and to allow a fuller description of the oxynitride system we have investigated a number of binary alloys in this study. Data from the magnetron-sputtered binary alloys are in good agreement (within the experimental error of ± 0.1 eV) with earlier work on unhydrogenated samples produced by RF sputtering. The lines of constant experimental optical bandgap for the ternary compound shown in figure 3 are roughly parallel to each other. The gradient of the lines becomes slightly more negative with increase in x and y, where the fastest rate of change of value of bandgap also occurs. The calculated values of bandgap also shown on the figure will be discussed in sections 7 and 8.

Experimentally obtained values of static refractive index $n(0)$, and dashed lines of constant experimental $n(0)$, are shown in the same format in figure 4. Again, the dots

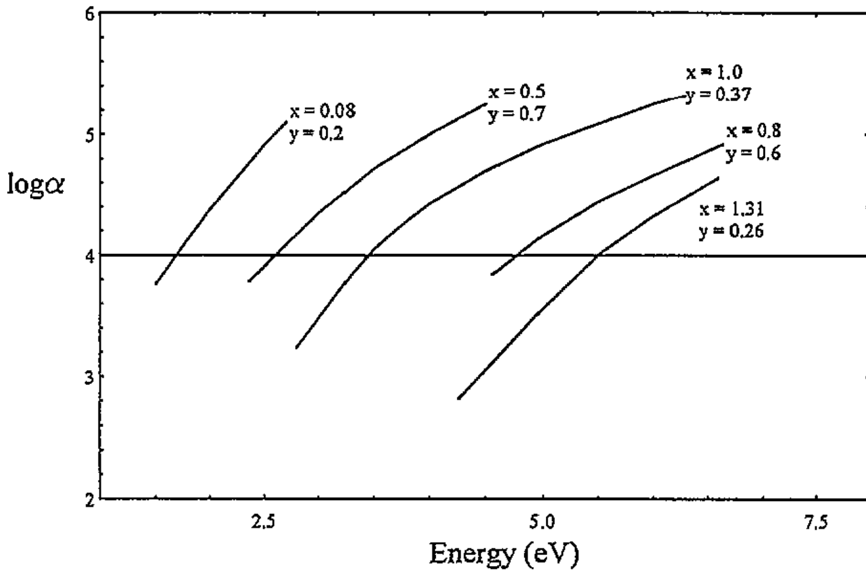

Figure 2. Absorption edges of several films of silicon oxynitride of various x, y. The horizontal line corresponds to the value of absorption at which the E_{04} bandgap is defined.

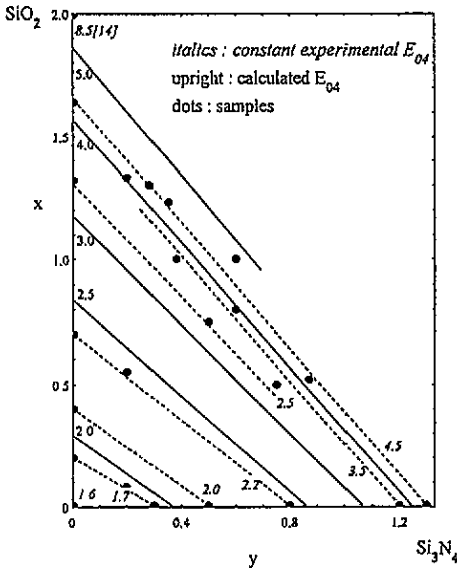

Figure 3. Optical bandgaps of a-SiO_xN_y as a function of composition x, y. Dots: sample compositions; dashed lines: lines of constant experimental bandgap; solid lines: lines of constant calculated bandgap, using Phillips scaling and assuming complete chemical order. Data for SiO_2 are from [17].

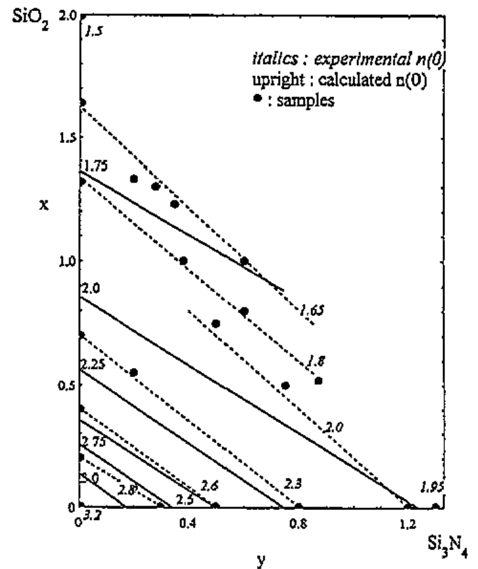

Figure 4. Refractive indices of a-SiO_xN_y as a function of composition x, y. Dots: experimental points; dashed lines: lines of constant experimental bandgap; solid lines: lines of constant calculated bandgap, using Phillips scaling and assuming complete chemical order.

represent the compositions of the samples studied. The values of $n(0)$ for the binary compound agree within experimental error (±0.02) with the values obtained previously

for RF sputtered samples [4, 5]. In addition, the lines of constant experimental $n(0)$ static refractive index are also roughly parallel to each other, again with slightly more negative gradient for larger x and y, but this time the fastest rate of change of $n(0)$ is at lower values of x and y. Once again the discussion of the calculated $n(0)$ is postponed until sections 7 and 8.

Optical tunability in the oxynitride system exists precisely because of differences in gradient of the set of lines of constant $n(0)$ and the set of lines of constant bandgap. This is shown in figure 5 where the experimental static refractive indices and bandgaps are plotted on the same diagram. The tunability does not exist at all for low values of x and y but increases with x and y. For example, by changing the composition from $x = \sim 1.3$–0.6, and $y = 0$–0.9, a change in bandgap ΔE_{04} of ~ 2 eV can be achieved with a constant refractive index $n(0)$ of 1.8. Similarly, by changing the composition from $x = 1.3$–0.5 and $y = 0$–0.7, a change in refractive index $\Delta n(0)$ of ~ 0.2 can be achieved with a constant bandgap E_{04} of 2.5 eV.

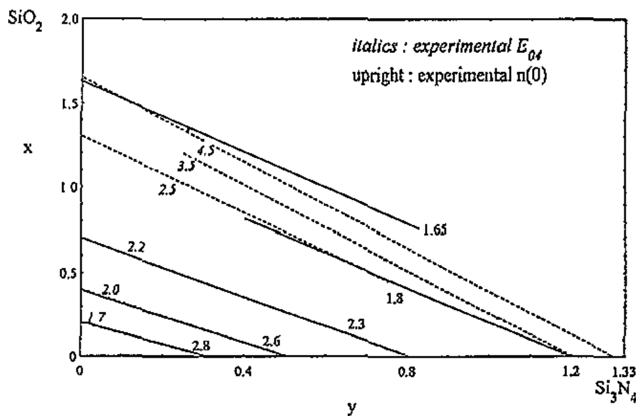

Figure 5. Overlay of experimentally determined refractive indices and optical bandgaps; data taken from figures 3 and 4.

7. Dielectric function and scaling theory

The behaviour of the dielectric function as a function of energy as the fundamental absorption edge is approached from the long-wavelength side contains information on the electronic transitions and is relatable to the electronic density of states. Thus the imaginary part ε_2 may be used to determine the fundamental optical gap, whereas the real part ε_1 gives rise to the refractive index. Since the measured dielectric functions of amorphous covalent alloys are all similar in shape as functions of energy, it is possible to describe them using scaling theory. In fact just two parameters are required to scale the dielectric functions of such alloys: firstly an amplitude scaling parameter C_1 and secondly an energy scaling parameter C_2. (In the case of silicon-based alloys it is the tetrahedral nature of the bonding which gives the similarity in the dielectric function.) The complex dielectric function of a reference material ε_s can then be scaled in the following way [7] to produce the complex dielectric function ε of any other system based on that reference material:

$$\varepsilon(E) - 1 = [\varepsilon_s(C_2E) - 1]. \quad (1)$$

The amplitude scaling parameter C_1 represents a relationship between the electron densities in the reference and 'sample', whereas the energy scaling parameter C_2 represents the difference in optical bandgap energy. The scaling parameters could be obtained empirically; however, relating them to physical dielectric parameters allows a deeper understanding of the systems under study.

The plasma sum rule is used to obtain a relationship between the two scaling constants, since this relates the integral ε_2 to an effective electron density N:

$$N = \frac{m}{2\pi^2 e^2 h^2} \int_0^\infty E\varepsilon_2(E)\,\mathrm{d}E. \tag{2}$$

Using the scaled form of ε_2 in this expression links C_1 and C_2 [7]:

$$C_2^2 = C_1(N_s/N) = C_1(E_{ps}/E_p)^2 \tag{3}$$

where N_s is the electron density of the reference material. We have also related the electron densities to their respective plasmon energies E_p, which are easier to measure.

As previously [4, 5, 7, 18] we choose to take the Penn gap model of Phillips [8] and van Vechten [9] as appropriate for silicon-based alloys, and apply it here to the ternary silicon oxynitride system to obtain a further relationship between the scaling constants. The Penn gap model is the isotropic free electron description of the density of states in a simple two-band system, so there is simply a single energy gap E_g surrounding the spherical Fermi surface.

The Phillips susceptibility χ is given by

$$n(0)^2 - 1 = \chi = \frac{E_p^2}{E_g^2} \tag{4}$$

where $\chi = \sum_j f_j \chi_j$ where the sum is over all bond types j, the independent bond model. Use of the scaling relation, equation (1), then gives an expression for C_1 in terms of the Penn gap and the electron density (or plasmon energy) [7]:

$$C_1 = E_{gs}^2 N / E_g^2 N_s \tag{5}$$

from which use of equation (3) gives

$$C_{2E_g} = E_{gs}. \tag{6}$$

8. Calculated optical properties

Refractive indices and optical bandgaps obtained from silicon using scaling by Phillips [7] and van Vechten [8], assuming complete chemical order, are shown by dashed lines in figures 3 and 4 respectively. The experimental dataset used for the reference was that of Piggins *et al* [19]. The agreement between the experimental and calculated data is good, although there are some discrepancies. Thus although the experimental and calculated refractive indices are very similar for a particular composition, the experimental bandgaps are slightly lower at low x and y, but much higher at high x and y, than the calculated

gaps. To understand the discrepancies it is necessary to consider further the bonding model used for the calculations.

The Penn gap itself (E_g) is formulated as the Pythagorean sum of the homopolar (covalent) and heteropolar (ionic) contributions, the homopolar part (E_h) coming from the Penn gap for pure covalent bonds as in elemental crystals. The heteropolar part (C) is due to the difference in coulombic potentials of the two ion cores. Thus the Penn gap is given by [8]

$$E_g^2 = E_h^2 + C^2.$$

It is recognized that there are some inadequacies in the model, in particular that the susceptibility is formulated as a linear sum of independent contributions from each bond type. Interaction between bonds occurs due to their partially ionic nature, and gives rise to charge transfer. The more ionic the system, the more important these effects are, giving rise to predictions of bandgap which are too low [7]. In the case of the binary alloys system we expect the ionicity effects to be consequential as far as bandgap calculations are concerned for values of $x > 1.5$ in SiO_x and $y > 1.0$ in SiN_y respectively [4, 5].

Despite the above caution, this approach is far simpler than the application of a tetrahedron model for instance [20], which although excellent for describing the dielectric functions of binary alloys [7, 20] would become horrendously complicated for a ternary system. Indeed the only experimental parameters required for an 'experimental' determination of the Penn gap are a measure of the electron density (usually obtained from plasmon energies) and refractive index. In addition an independent bond model gives respectable values (within 10%) of the real and imaginary parts of the dielectric functions of, for example, the silicon nitride system [7] at the low energies, where the dielectric constant is not changing fast.

Finally, it should be noted that a void fraction has been intrinsically included in the model by the use of a reference sample also prepared by sputtering. This is correct procedure since it is known experimentally for various forms of silicon, from small-angle scattering data, that the void fraction is of the order of 5% for sputtered, unhydrogenated material [21]. The effect of including a 5% void fraction would be to lower the value of refractive index by $\sim$ 5%, but leave E_{04} unchanged. However, use of a reference sample also prepared by sputtering means that there is no need to adjust either $n(0)$ or the bandgap further. In fact, the refractive index predictions of the independent bond model are good throughout the composition range of the ternary compound. As discussed above, it is the bandgap predictions which suffer as a result of this model.

9. Summary

We have shown that magnetron-sputtered silicon oxynitride is chemically ordered, with very few Si–Si bonds occurring in samples with compositions close to stoichiometry. The binary members of the system show optical properties which are similar to their RF-sputtered counterparts. Tailoring a specified bandgap with varying refractive index (or specified refractive index with tunable bandgap) is achievable in the ternary compound but only within the higher nitrogen and/or oxygen composition range.

Scaling theory using an independent bond model is useful for predicting the optical properties of this tetrahedral ternary system: the simplicity of this approach makes it very attractive for complex systems when compared to, for example, the tetrahedron model.

Acknowledgments

The authors would like to acknowledge the support of the SERC SRS which made this work possible, and Mr G Hall, LUT, for sample preparation.

References

[1] Hubner K 1980 *J. Non-Cryst Solids* **35 & 36** 1011
[2] Holzenkampfer E, Stuke J and Fischer R 1982 *Proc. 4th European Community Photovoltaic Solar Energy Conf. (Stresa, Italy, 1982)* (Dordrecht: Reidel) p 778
[3] Haga K, Yamamoto K, Kumano M and Watanabe H 1986 *Japan. J. Appl. Phys. Suppl. 2* **25** L39
[4] Bayliss S C and Gurman S J 1991 *J. Non-Cryst. Solids* **127** 174
[5] Singh A, Bayliss S C, Gurman S J and Davis E A 1992 *J. Non-Cryst. Solids* **142** 113
[6] Howson R P and Hall G W 1991 *Proc. 8th IPAT (Brussels)* (CEP Consultants Ltd) p 128
[7] Gurman S J 1992 *J. Non-Cryst. Solids* **143** 207
[8] Phillips J C 1968 *Phys. Rev. Lett.* **20** 550
[9] van Vechten J A 1969 *Phys. Rev.* **187** 1007
[10] Elam W T, Kirkland J P, Neiser R R and Wolf P D 1988 *Phys. Rev.* B **38** 26
[11] Viegele W J 1973 *At. Data* **5** 51
[12] Morrell C, Campbell J C, Diakun G P, Dobson B R, Greaves G N and Hasnain S S 19 *EXAFS Users' Manual* (Daresbury: SERC)
[13] Gurman S J, Binsted N and Ross I 1984 *J. Phys. C: Solid State Phys.* **17** 143
[14] Cisneros J I, Rego G B, Tomyiama M, Bilac S, Gonclaves J M, Rodriguez A E and Arguello Z P 1983 *Thin Solid Films* **100** 155
[15] Bustarret E, Ligeon M and Ortega L 1992 *Solid State Commun.* **83** 461
[16] Canham L T 1990 *Appl. Phys. Lett.* **57** 1046
[17] Holzenkampfer E, Richter F W, Stuke J and Voget-Grote V 1979 *J. Non-Cryst. Solids* **32** 327
[18] Bayliss S C, Gurman S J, Asal R and Hall D 1991 *J. Non-Cryst. Solids* 894
[19] Piggins N, Bayliss S C, Davis E A and Shen J 1989 *J. Phys.: Condens. Matter* **1** 8111
Davis E A, Piggins N and Bayliss S C 1987 *J. Phys. C: Solid State Phys.* **20** 4415
[20] Yin Z and Smith F W 1990 *Phys. Rev.* B **42** 2658 and 3666
[21] Mahan A H, Chen Y, Williamson D L and Mooney G D 1991 *J. Non-Cryst. Solids* **137 & 138** 65